Oxidation of Methanol on 2nd and 3rd Row Group VIII Transition Metals (Pt, Ir, Os, Pd, Rh, and Ru): Application to Direct Methanol Fuel Cells

Jeremy Kua and William A. Goddard III*

Contribution from the Materials and Process Simulation Center, Beckman Institute (139-74), Division of Chemistry and Chemical Engineering, California Institute of Technology, Pasadena, California 91125

Received December 22, 1998. Revised Manuscript Received September 24, 1999

Abstract: Using first principles quantum mechanics [nonlocal density functional theory (B3LYP)], we calculated the 13 most likely intermediate species for methanol oxidation on clusters of all 2nd and 3rd row Group VIII transition metals for all three likely binding sites (top, bridge, and cap). This comprehensive set of binding energies and structures allows a detailed analysis of possible reaction mechanisms and how they change for different metals. This illustrates the role in which modern quantum chemical methods can be used to provide data for combinatorial strategies for discovering and designing new catalysts. We find that methanol dehydrogenation is most facile on Pt, with the hydrogens preferentially stripped off the carbon end. However, water dehydrogenation is most facile on Ru. These results support the bifunctional mechanism for methanol oxidation on Pt−Ru alloys in direct methanol fuel cells (DMFCs). We find that pure Os is capable of performing both functionalities without cocatalyst. We suggest that pure Os be examined as a potential catalyst for low overpotential, highly dispersed catalyst DMFCs. Pathways to form the second C−O bond differ between the pure metals (Pt and Os) in which $(CO)_{ads}$ is probably activated by $(OH)_{ads}$ and the Pt−Ru binary system in which $(COH)_{ads}$ is probably activated by O_{ads}. For all cases we find that formation of $(COOH)_{ads}$ is an important precursor to the final dehydrogenation to desorb CO_2 from the surface.

1. Introduction

Fuel cells are electrochemical cells in which both fuel and oxidant are fed in a continuous supply to the electrodes. They are attractive sources of electrical power since the production of electrical energy can be maintained as long as the reactants are supplied to the electrodes. This concept was first proposed in 1839 by Sir W. R. Grove, and direct conversion of chemical to electric energy in a hydrogen/oxygen fuel cell was demonstrated. Although hydrogen/oxygen fuel cells are used in spaceships, wider applications in traction-based vehicles (for example, electric cars) are limited by unsolved problems such as transport and storage of hydrogen. Liquid fuels would solve this problem; however, extracting molecular hydrogen from a liquid fuel requires a reformer. This greatly increases the overall cost of the cell, reducing the fuel conversion efficiency.

An alternative to H_2 is the use of a liquid fuel such as methanol supplied directly to the anode and electrooxidized to CO_2. Indeed, recent results for model direct methanol fuel cells (DMFCs) show that critical performance parameters for commercial use are now achievable with modern catalytic formulations and cell designs.[1] A simple schematic of the DMFC is shown in Figure 1. The fuel (methanol and water) is passed through the anode, and the oxidant (O_2 in air) flows through the cathode. The two electrodes are separated by a proton-exchange membrane such as Nafion. Platinum-based electrodes demonstrate the highest catalytic activity and cleanest combustion products. Since engines operate at high temperatures, this whole system will be in an "oven-like" setting. The design and construction of high-performance DMFCs is already undergoing optimization.[1]

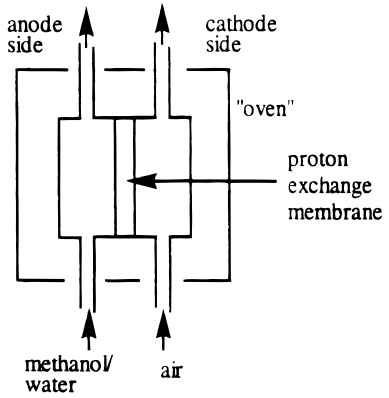

Figure 1. Schematic of a direct methanol fuel cell.

An obvious advantage of the DMFC over the internal combustion engines is to avoid the environmental damage caused by the latter. The alternative use of batteries could, in principle, operate a vehicle without unwanted emissions; however, current batteries also have environmental problems and require constant recharging. The DMFC, on the other hand, can provide a continuous supply of electrical energy as long as there is available fuel. Renewable liquid fuel alternatives such as methanol also allow use of the current infrastructure for petroleum.

However, the DMFC does have disadvantages, the primary problem being a low power density. High over-potentials at the anode catalyst combined with the necessity of using low temperatures severely reduces the conversion efficiency. Thus,

* To whom correspondence should be addressed (wag@wag.caltech.edu).

(1) Hogarth, M.; Christensen, P.; Hamnett, A.; Shukla, A. *J. Power Sources* **1997**, *69*, 113.

10.1021/ja9844074 CCC: $18.00 © 1999 American Chemical Society
Published on Web 11/12/1999

high loadings of noble metals are required to enhance the performance of the anode, increasing costs. In addition, the membrane properties need to be improved with respect to water balance sensitivity (six protons at the anode produced per methanol molecule) and inhibition of methanol crossover. Diffusion of methanol across the membrane leads to depolarization of the cell and loss of activity.

Recently, advances have been made in two significant areas: (1) the use of solid polymer electrolyte (SPE) technology now allows increased operating temperatures, thereby improving efficiency[2] and (2) improved electrocatalysts have been identified that increase reaction activity, allowing reduction of the noble metal loading. This decreases the cost and generates higher power densities. This paper will focus on the latter area.

The progress in developing improved DMFCs has been hindered by the lack of a detailed reaction mechanism. Relevant mechanistics were discussed by Leger and Lamy,[3] and recently reviewed by Hamnett,[4] while Parsons and VanderNoot[5] provide an earlier review of fuel cell research.

Section 2 summarizes the current understanding of the catalytic oxidation of methanol on platinum black and platinum-based electrodes, and discusses the bifunctional mechanism for Pt−Ru alloys. Section 3 presents details of our calculations which use a finite cluster suggested by the interstitial electron model (IEM).[6] Sections 4 and 5 present the results of calculations for the intermediates involved in this reaction on the 2nd and 3rd row Group VIII transition metals (Pt, Ir, Os, Pd, Rh, and Ru). In particular, these results support the bifunctional mechanism of Pt−Ru. They also suggest that the pure metal Os is capable of performing both functions of the bifunctional mechanism, without cocatalyst. Section 6 presents the conclusions.

2. Review of Mechanistic Understanding for Direct Methanol Oxidation

There are several different plausible pathways for the oxidation of methanol. Water is required for the overall conversion of methanol to carbon dioxide

$$CH_3OH + OH_2 \rightarrow CO_2 + 6H^+ + 6e^- \quad (1)$$

Methanol adsorbed on the electrode surface can undergo successive dehydrogenation, as indicated in steps 2−5. However, the exact structure of the adsorbed intermediates is unknown except for $(CO)_{ads}$.

$$(CH_3OH)_{ads} \rightarrow (CH_3O)_{ads} + H^+ + e^- \quad (2)$$

$$(CH_3O)_{ads} \rightarrow (CH_2O)_{ads} + H^+ + e^- \quad (3)$$

$$(CH_2O)_{ads} \rightarrow (CHO)_{ads} + H^+ + e^- \quad (4)$$

$$(CHO)_{ads} \rightarrow (CO)_{ads} + H^+ + e^- \quad (5)$$

Our computational results (vide infra) suggest which particular isomers are the adsorbed species. Water may also dehydrogenate successively to form adsorbed OH and O atom as in steps 6 and 7.

$$(OH_2)_{ads} \rightarrow (OH)_{ads} + H^+ + e^- \quad (6)$$

$$(OH)_{ads} \rightarrow (O)_{ads} + H^+ + e^- \quad (7)$$

Formation of a second C−O bond is then required to remove $(CO)_{ads}$ from the surface in the form of CO_2 as in

$$(CO)_{ads} + O_{ads} \rightarrow CO_2 \quad (8a)$$

Equation 8a assumes complete dehydrogenation for both CH_3OH and H_2O takes place to form CO_{ads} and O_{ads} which then forms CO_2, which desorbs from the surface. However, it is possible that partially dehydrogenated species could recombine and then dehydrogenate (either simultaneously or in a successive step) to form CO_2 as in

$$(CO)_{ads} + (OH)_{ads} \rightarrow (COOH)_{ads} \rightarrow CO_2 + H_{ads} \quad (8b)$$

The recombination of partially dehydrogenated species could also produce compounds such as HCOOH, $HCOOCH_3$, and $CH_2(OCH_3)_2$, all of which have been observed experimentally.[7]

2.1. Experimental Observations. It has long been known that Pt−Ru alloy electrodes increase the electrocatalytic activity compared to pure Pt electrodes.[8,9] Many recent advances in experimental techniques have contributed to elucidating the reaction mechanism. Recently on-line Fourier transform infrared (FTIR) spectroscopy[7] and real-time mass spectrometry[10] have been used to detect intermediates formed at higher operating temperatures. [Previous studies had been performed only at room temperature.[11]] Low-energy ion scattering (LEIS), under ultra-high vacuum (UHV) conditions, has been used to determine the surface compositions of various polycrystalline Pt−Ru bulk alloys[12] allowing kinetic studies as a function of temperature.[13] In situ X-ray absorption studies have been performed to characterize the Pt−Ru phases.[14] Differential electrochemical mass spectrometry (DEMS) has been used to compare the activity of Pt−Ru with pure Pt and pure Ru.[15] Structural effects and reactivity on different single-crystal faces of platinum have been compared,[16] as have the effects of using bulk Pt, Pt particles, and carbon-black-supported Pt−Ru electrodes.[17]

It is known that methanol oxidation on platinum is structure-sensitive,[18] but the issue of size effects is unresolved. The Oxford group suggested an optimum diameter of 2 nm;[19] however, other studies do not find evidence for size effects, even for particles as small as 1.4 nm.[20]

(2) Scherer, G. G. *Ber. Bunsen-Ges. Phys. Chem.* **1990**, *94*, 1008.
(3) Leger, J.-M.; Lamy, C. *Ber. Bunsen-Ges. Phys. Chem.* **1990**, *94*, 1021.
(4) Hamnett, A. *Catal. Today* **1997**, *38*, 445.
(5) Parsons, R.; VanderNoot, T. *J. Electroanal. Chem.* **1988**, *257*, 9.
(6) Kua, J.; Goddard, W. A., III *J. Phys. Chem. B* **1998,** *102*, 9481.
(7) Lin, W. F.; Wang, J. T.; Savinell, R. F. *J. Electrochem. Soc.* **1997**, *144*, 1917.
(8) Bockris, J. O.; Wroblowa, H. *J. Electroanal. Chem.* **1964**, *7*, 428.
(9) Petry, O. A.; Podlovchenko, B. I.; Frumkin, A. N.; Hira, L. *J. Electroanal. Chem.* **1965**, *10*, 253.
(10) Wasmus, S.; Wang, J.-T.; Savinell, R. F. *J. Electrochem. Soc.* **1995**, *142*, 3825.
(11) Yamanaka, I.; Otsuka, K. *Electrochim. Acta* **1989**, *34*, 211
(12) Gasteiger, H. A.; Markovic, N.; Ross, P. N., Jr.; Cairns, E. J. *J. Phys. Chem.* **1994**, *98*, 617.
(13) Gasteiger, H. A.; Markovic, N.; Ross, P. N., Jr.; Cairns, E. J. *J. Electrochem. Soc.* **1994**, *141*, 1795.
(14) McBreen, J.; Mukerjee, S. *J. Electrochem. Soc.* **1995**, *142*, 3399.
(15) Krausa, M.; Vielstich, W. *J. Electroanal. Chem.* **1994**, *379*, 307.
(16) Xia, X. H.; Iwasita, T.; Ge, F.; Vielstich, W. *Electrochim. Acta* **1996**, *41*, 711
(17) Munk, J.; Christensen, P. A.; Hamnett, A.; Skou, E. *J. Electroanal. Chem.* **1996**, *401*, 215.
(18) Lamy, C.; Leger, J.-M.; Clavilier, J.; Parsons, R. *J. Electroanal. Chem.* **1983**, *150*, 71.
(19) Kennedy, B. J.; Hamnett, A. *J. Electroanal. Chem.* **1990**, *283*, 271.

The confirmation that $(CO)_{ads}$ is the poisoning species [and not $(COH)_{ads}$ or $(CHO)_{ads}$] was made possible by electromodulated infrared reflectance spectroscopy (EMIRS).[21] A chronological review of electrooxidation of CO on polycrystalline Pt has been provided by Beden and Lamy.[22]

Recent experiments using combinatorial screening of electrochemical catalysts have identified ternary and quaternary alloys with higher activity than Pt−Ru.[23] The alloy with the best catalytic activity reported is $Pt_{0.44}Ru_{0.41}Os_{0.10}Ir_{0.05}$. The observation that Ir and Os can serve as promoters raises the question of what role is played by each different metal in the oxidation reaction.

2.2. Bifunctional Mechanism of Pt−Ru. The bifunctional mechanism of Pt−Ru was first presented by Watanabe and Motoo.[24] According to this mechanism, Pt is responsible for catalyzing the dehydrogenation of methanol. On pure Pt, this reaction is poisoned because of the formation of $(CO)_{ads}$ after complete dehydrogenation of methanol. The removal of CO is facilitated by Ru, which may act by weakening the Pt−CO bond, and/or by promoting the oxidation of CO to CO_2 via activation of water in an adjacent site to facilitate the formation of the second C−O bond. The onset potential of forming CO_2 on Pt−Ru (0.220 V vs RHE) is lower than that on Pt-black (0.325 V vs RHE).[7] This has been attributed to the ability of Ru to adsorb OH at lower potentials.[25] Pure Pt decomposes water at a high potential of 0.8 V vs RHE, whereas on pure Ru, the potential required is only 0.2 V vs RHE.[12]

2.3. Previous Computational Approaches. 2.3.1. Semiempirical MO Calculations. Using semiempirical molecular orbital calculations on cluster models, Anderson[26] has studied the interaction of $(CO)_{ads}$ and $(OH)_{ads}$ on Pt(111) using a bilayer Pt_{18} cluster to model two reactions: (1) the dehydrogenation of water to form $(OH)_{ads}$ and (2) the interaction of $(CO)_{ads}$ and $(OH)_{ads}$ to form the second C−O bond. These calculations used a modification of extended Huckel theory in which an empirical two-body nuclear−nuclear term is added to improve geometries and energetics. This is called Atom Superposition and Electron Delocalization Molecular Orbital (ASED-MO) theory. Their results suggest that reaction 8b has a barrier of 22.6 kcal/mol. However, ASED-MO calculations yield binding energies that are far too high. For example, ASED-MO leads to a binding energy for H_2O of 41.7 kcal/mol compared to 12 kcal/mol from experiment,[27]a binding energy for CO of 56.7 kcal/mol compared to 43 kcal/mol from experiment experiment,[28] see section 4.2.5a, and a binding energy for OH of 90.4 kcal/mol compared to 47 kcal/mol from experiment.[29]With binding energies too high by 30, 14, and 43 kcal/mol, it is doubtful that the calculated barriers are reliable. As discussed in Section 4, DFT B3LYP calculations lead to binding energies (kcal/mol) of 16.0 (H_2O), 41.9 (CO), and 40.8 (OH) kcal/mol, which are off by 4, 1, and 6 kcal/mol, respectively, from experiment.

A further study done on mixed Pt−Ru clusters[30] suggested that the adsorption of OH was stronger on Ru (binding energy of 122 kcal/mol) than Pt. The dehydrogenation of OH_2 was then studied on a series of $Pt_{17}M$ clusters for M atoms in periods 4−6 of the Periodic table.[31] In these studies, only the on-top sites were considered for the adsorbed species. We show below that bridging sites and cap sites also play a role.

2.3.2. First Principles Calculations. Recent studies using first principles gradient-corrected density function theory (DFT) (BP86) examined the chemisorption of CO on Pt−Pt, Pt−Ni, and Pt−Ru dimers.[32] They found binding energies (kcal/mol) of 33, 5, and −5, respectively, indicating that bridged CO binds weakest to Pt−Ru.

Other computational work focused on the binding of CO to Pt using a variety of computational approaches and different levels of theory. For example, restricted Hartree−Fock (RHF) on[33] Pt_4 leads to a binding energy of 27.0 kcal/mol (on-top site) [complete active space self-consistent field (CASSCF) on the same cluster gave the same structural parameters but the binding energy was not reported], DFT-GGA on[34] Pt_{10} leads to a binding energy for CO of 41.8 kcal/mol (on-top site), and gradient corrected DFT on Pt with periodic boundary conditions[35] leads to a binding energy of 33.4 kcal/mol (on-top site).

Thus the various cluster calculations suggest an on-top site with energies 16, 1, and 10 kcal/mol weaker than the experimental value of 43 kcal/mol. Our calculations (vide infra) lead to a cap site with a bond energy of 41.9 kcal/mol.

3. Computational Strategy

To provide a more detailed understanding of the basic mechanistic issues, we will separately consider three aspects of the catalytic reaction: (1) dehydrogenation of methanol, (2) dehydrogenation of water, and (3) formation of oxidized species to finally yield desorbed CO_2.

We examined these reaction steps for six 2nd and 3rd row Group VIII transition metals. This includes Pt and Ru, the two basic ingredients established to exhibit the bifunctional mechanism, and includes Ir and Os, which have been demonstrated to act as promoters in Pt−Ru catalysts. We will compare the activity of each of these metals by examining the thermodynamics for each intermediate involved in the reaction.

Our strategy here is to use a consistent accurate level of theory on all plausible reaction intermediates (we considered over 13) at all plausible surface sites (we considered top, bridge, and cap sites) on all six transition metals. This sort of comprehensive data at a consistent level of accuracy has never before been available. Using these data we have considered the plausible reaction mechanisms. We have examined the reaction path and barrier for several cases to estimate the magnitude of the likely barriers, but we have not done systematic studies of the barriers. Instead we focus on comparing data that could be useful in discovering new candidates for catalysts and for designing experimental studies.

3.1. The M_8 Cluster Model. On the basis of a series of computations for the electronic structures of Pt_N clusters, we developed the IEM for bonding that explained the details of the optimum electron states in terms of a simple orbital model.[6] The IEM model suggests that the surface atoms of the (111) surface of bulk Pt have a valence $6s^1 5d^9$ electronic configuration. This suggests that to mimic the surface

(20) Watanabe, M.; Saegusa, S.; Stonehart, P. *J. Electroanal. Chem.* **1989**, *271*, 213.
(21) Beden, B.; Lamy, C.; Bewick, A.; Kunimatsu, K. *J. Electroanal. Chem.* **1981**, *121*, 343.
(22) Beden, B.; Lamy, C. *Electrochim. Acta* **1990**, *35*, 691.
(23) Reddington, E.; Sapienza, A.; Gurau, B.; Viswanathan, R.; Saragapani, S.; Smotkin, E. S.; Mallouk, T. E. *Science* **1998**, *280*, 1735.
(24) Watanabe, M.; Motoo, S. *J. Electroanal. Chem.* **1975**, *60*, 275.
(25) Iwasita, T.; Nart, F. C.; Vielstich, W. *Ber. Bunsen-Ges. Phys. Chem.* **1990**, *94*, 1030.
(26) Anderson, A. B.; Grantscharova, E. *J. Phys. Chem.* **1995**, *99*, 9143.
(27) Thiel, P. A.; Madey, T. E. *Surf. Sci. Rep.* **1987**, *7*, 211.
(28) Yeo, Y. Y.; Vattuone, L.; King, D. A. *J. Chem. Phys.* **1997**, *106*, 392.
(29) Williams, W. R.; Marks, C. M.; Schmidt, L. D. *J. Phys. Chem.* **1992**, *96*, 5922.
(30) Anderson, A. B.; Grantscharova, E. *J. Phys. Chem.* **1995**, *99*, 9149.
(31) Anderson, A. B.; Grantscharova, E.; Seong, S. *J. Electrochem. Soc.* **1996**, *143*, 2075.
(32) Mitchell, P. C. H.; Wolohan, P.; Thompsett, D.; Cooper, S. J. *J. Mol. Catal. A* **1997**, *119*, 223.
(33) Illas, F.; Zurita, S.; Marquez, A. M.; Rubio, J. *Surf. Sci.* **1997**, *376*, 379.
(34) Watwe, R. M.; Spiewak, B. E.; Cortright, R. D.; Dumesic, J. A. *Catal. Lett.* **1998**, *51*, 139.
(35) Hammer, B.; Nielsen, O. H.; Norksov, J. K. *Catal. Lett.* **1997**, *46*, 31.

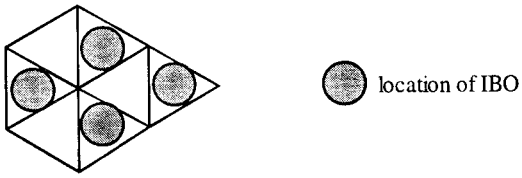

Figure 2. The model M_8 cluster. In Pt_8 this cluster leads to an s^1d^9 configuration for all low-lying electronic states.

chemistry for metal surfaces, a cluster model should lead to the s^1d^9 electronic configurations on each atom while providing internal binding sites prototypical for all three sites of Pt (111).

This suggested[6] the Pt_8 cluster shown in Figure 2 as the most economical choice satisfying these two properties. This M_8 model cluster was used previously[36] to study the thermodynamics of two reactions: (1) the dehydrogenation of methane on Pt(111) and (2) the chemistry of ethylene on Pt(111).[36] In both cases the results were consistent with available experimental data.

In this paper we apply the same methodology to study the DMFC chemistry on six metals (Pt, Ir, Os, Pd, Rh, and Ru). Pt, Ir, Pd, and Rh are face-center-cubic (fcc) metals, so that the M_8 cluster models the (111) surface. Os and Ru are both hexagonal-closed-packed (hcp), so that the M_8 cluster models the (0001) surface. This is a reasonable choice since X-ray diffraction (XRD) suggests that the platinum alloys active in methanol oxidation are all in the fcc phase[14] and that the closed-packed surface (111) dominates.

3.2. Details for QM Computations. Calculations were carried out with the nonlocal DFT (generalized gradient approximation) including exact exchange. Specifically we use the B3LYP method which combines the exact Hartree−Fock (HF) exchange operators with the Slater local exchange functional[37] using the parameters referred to as Becke3.[38] In addition, we used the Becke nonlocal gradient correction,[39] the Vosko−Wilk−Nusair exchange functional,[40] and the Lee−Yang−Parr local and nonlocal correlation functional.[41]

All calculations were carried out using the Jaguar program.[42,43] The metals were described using the Hay and Wadt core-valence relativistic effective-core potential (ECP) with 18 explicit electrons for Pt, Pd; 17 electrons for Ir, Rh; and 16 electrons for Os, Ru[44] (denoted LACVP in Jaguar). This is a nonlocal ECP using angular momentum projection operators to enforce the Pauli principle.[45−48] All electrons were considered for carbon, oxygen, and hydrogen using the 6-31G** basis set.

3.3. Spin States. The various spin states were calculated as pure spin states (not unrestricted Hartree−Fock). The optimum spin of the metal−adsorbate complex is determined by separate calculations of all low-lying spins, where in each case the geometric structure for each adsorbate on the metal surface was fully optimized. However, the M−M bonds in each cluster were frozen at their bulk distances (Pt 2.775 Å; Ir 2.714 Å; Os 2.734 Å; Pd 2.750 Å; Rh 2.689 Å; Ru 2.706 Å). This is because we consider that the real catalyst particles are sufficiently large to enforce this structure.

For the various M_8 clusters we calculated the various low-lying spin and base all energetics on the calculated ground spin states, S_M (Table 1). In each case except Pd the electronic structure is consistent with the IEM, which suggests s^1d^{n-1} character in the surface atoms. The IEM suggests that the maximum spin of the cluster is $S = 8[10 - (n\text{-}1)]/2$, where n is the number of valence electrons. This predicts spins of $S = 12$, 8, and 4 for columns 8, 9, and 10. Indeed for Ir the ground state has $S = 8$. For the other metals, there is sufficient d−d overlap that some electrons in the high-lying d-orbitals spin pair, leading to lower net spins. For example, the ground state of Pt_8 is the $S = 3$ state, 1.4 kcal/mol lower in energy than the $S = 4$ state.[6] Pd_8 is anomalous in that the Pd_8 cluster has almost all d-electrons spin paired. This is because the ground state of the Pd atom is d^{10}, whereas the other metals have s^1d^{n-1} atomic ground states.

Table 1. Reference Energies and Assigned Heats of Formation of Reference Compounds

ref	exptl H_f (kcal/mol)	ref energies (hartrees)
Pt_8 ($S = 3$)	0	$E_0(Pt_8) = -953.25726$
Ir_8 ($S = 8$)	0	$E_0(Ir_8) = -837.40601$
Os_8 ($S = 10$)	0	$E_0(Os_8) = -728.00941$
Pd_8 ($S = 1$)	0	$E_0(Pd_8) = -1013.98567$
Rh_8 ($S = 7$)	0	$E_0(Rh_8) = -875.98723$
Ru_8 ($S = 11$)	0	$E_0(Ru_8) = -750.83465$
H_2	0	$E_0(H) = -0.58927$
CH_4	−17.9[a]	$E_0(C) = -38.13845$
OH_2	−57.8[a]	$E_0(O) = -75.14908$

[a] Reference 49.

For the metal−adsorbate clusters, we also calculated the various low-lying spin states and base all energetics on the ground spin state S_{a+M}. The previous results[36] on C_xH_y/Pt_8 showed that each unpaired electron of the C_xH_y forms a localized covalent bond to an unpaired d-orbital of the Pt_8. Thus we expect the ground spin state to satisfy the formula $S_{a+M} = S_M - b/2$, where b is the number of bonds formed between the adsorbate and the surface. Occasionally (especially in 3-fold cap sites, and for some oxygen-based adsorbates) bonding the adsorbate leads to unpairing of a spin-paired d-orbital, resulting in $S_{a+M} = S_M - b/2 + 1$. Formally this corresponds to forming a covalent bond to the excited state of M_8 having a spin higher by 1.

4. Results for Pt

We summarize in this section the results for Pt since all good DMFC catalysts involve Pt and since there is more experimental data with which to compare the theory. Section 5 will compare the results for all six metals. We consider separately three parts of the reaction: (1) dehydrogenation of methanol, (2) dehydrogenation of water, and (3) formation of the second C−O bond. For each of these reactions, we calculated the equilibrium structures of ∼13 intermediates at each of the three sites on each of the six metals (Pt, Ir, Os, Pd, Rh, and Ru).

4.1. Calculation of Heats of Formation. For simplicity in comparing a large number of adsorbates on a number of metals and sites, we choose to reference our calculated energetics for the minimized structures with experimental heats of formation at room temperature. This is not rigorous. To compare energetics at room temperature, we should correct all calculated numbers for zero-point energy and for changes in the enthalpy to room temperature. Such corrections will lead to changes in the final heat of formation of a few kilocalories per mole, which are expected to be nearly the same for adsorbates at the same site of the various metals. Hence, in the interests of comprehensive results for many cases, we neglect these corrections here.

For convenience in considering the thermodynamics of these reactions, we convert the calculated metal−adsorbate energetics into heats of formation for each chemisorbed species. To calculate the heats of formation, we must choose an appropriate ensemble of reference compounds (one for each element). We chose the reference compounds as follows: (1) M_8 in the ground state ($S = 3$ for Pt_8) (2) gas-phase H_2, (3) gas-phase methane, and (4) gas-phase water.

(36) Kua, J.; Goddard, W. A., III *J. Phys. Chem. B* **1998**, *102*, 9492.
(37) Slater, J. C. *Quantum Theory of Molecules and Solids*, Vol. 4: *The Self-Consistent Field for Molecules and Solids*, McGraw-Hill: New York, 1974.
(38) Becke, A. D. *J. Chem. Phys.* **1993**, *98*, 5648.
(39) Becke, A. D. *Phys. Rev. A* **1988**, *38*, 3098.
(40) Vosko, S. H.; Wilk, L.; Nusair, M. *Can. J. Phys.* **1980**, *58*, 1200.
(41) Lee, C.; Yang, W.; Parr, R. G. *Phys. Rev. B* **1988**, *37*, 785.
(42) Jaguar 3.0, Schrodinger, Inc.: Portland, OR, 1997.
(43) Greeley, B. H.; Russo, T. V.; Mainz, D. T.; Friesner, R. A.; Langlois, J.-M.; Goddard, W. A., III; Honig, B. *J. Am. Chem. Soc.* **1994**, *116*, 11875.
(44) Hay, P. J.; Wadt, W. R. *J. Phys. Chem.* **1985**, *82*, 299.
(45) Goddard, W. A., III *Phys. Rev.* **1968**, *174*, 659.
(46) Kahn, L. R.; Goddard, W. A., III *J. Chem. Phys.* **1972**, *56*, 2685.
(47) Melius, C. F.; Goddard, W. A., III *Phys. Rev. A* **1974**, *10*, 1528.
(48) Melius, C. F.; Olafson, B. O.; Goddard, W. A., III *Chem. Phys. Lett.* **1974**, *28*, 457.

Table 2. Calculated Energies, Heats of Formation, and Spin States of CH_xO/Pt_8 Clusters

adsorbate on Pt_8	spin	site	binding energy (kcal/mol)	δH_f (kcal/mol)
CH_3OH	3	top	14.95	−63.40
OCH_3	7/2	top	25.04	−23.62
OCH_3	7/2	bridge	23.73	−22.31
CH_2OH	5/2	top	65.65	−63.47
CH_2O	2	bridge	9.62	−32.94
CHOH	2	bridge	84.84	−53.28
CHO	5/2	top	62.72	−46.25
COH	5/2	cap	121.16	−62.10
CO	3	cap	41.88	−55.64
CO	3	bridge	41.64	−55.40
CO	3	top	24.90	−38.66
H	5/2	cap	67.23	−11.38

Table 3. Optimized CH_xO Ground Spin States

fragment	spin	fragment	spin
CH_3OH	0	CHO	1/2
OCH_3	1/2	COH	1/2
CH_2OH (anti)	1/2	CO	0
CH_2O	0	H	1/2
CHOH (trans)	0		

The calculated energies of the reference compounds are shown in Table 3. Heats of formation for methane and water are taken from gas-phase experimental values. The procedure used to calculate heats of formation is as follows.

4.1.1. Pt Cluster. Since $H_f(Pt_8) = 0$, the *reference energy* for Pt_8 is $E_0(Pt_8) = -953.25726h$.

4.1.2. H Atom. Since $H_f(H_2) = 0$, the *reference energy* for hydrogen is $E_0(H) = -0.58927$ hartree (half the calculated value for an isolated H_2 molecule).

4.1.3. C Atom. The *reference energy* of carbon, $E_0(C)$, is derived from

$$C_{atom} + 2H_2 \rightarrow CH_4 \quad (8)$$

Since[49] $\Delta H_f(CH_4) = -17.9$ kcal/mol $= -0.02852h$, we obtain

$$E(CH_4) = -40.52405 = -0.02852h + E_0(C) + 4E_0(H) \quad (9)$$

Thus, $E_0(C) = -38.13845h$.

4.1.4. O Atom. The *reference energy* of oxygen, $E_0(O)$, is derived from

$$O_{atom} + H_2 \rightarrow OH_2 \quad (10)$$

Since[49] $\Delta H_f(H_2O) = -57.8$ kcal/mol $= -0.09211h$, we obtain

$$E(OH_2) = -76.41973 = -0.09211h + E_0(O) + 2E_0(H) \quad (11)$$

thus $E_0(O) = -75.14908h$.

4.1.5. H_{ads}. Using Pt_8 we calculate binding energies of 67.2 kcal/mol for η_3H/Pt_8 (cap site), 65.5 kcal/mol for η_2H/Pt_8 (bridge site), and 66.7 kcal/mol for η_1H/Pt_8 (on-top site). This suggests that H prefers the cap site on Pt (in agreement with experiment). The calculated desorption enthalpy to obtain gas-phase H_2 is 11.38 kcal/mol per adsorbed H. This compares with 10.6 kcal/mol from low-energy electron diffraction (LEED) and thermal desorption spectroscopy (TDS).[50] Similar techniques yield desorption enthalpies (per adsorbed H) of 12.6 kcal/mol for Ir(111),[51] 10.6 kcal/mol for Pd(111),[52] 10.1 kcal/mol for Rh(111),[53] and 9.5 kcal/mol for Ru(0001).[54] Since the variation of energy is small, we will use the same value of −11.38 kcal/mol calculated for $\delta H_f(H_{ads})$ on Pt for all the metals. This simplifies the comparison of different adsorbates on these various metals.

Table 4. Calculated Energies, Heats of Formation, and Spin States of OH_x/Pt_8 Clusters

adsorbate on Pt_8	spin	site	binding energy (kcal/mol)	δH_f (kcal/mol)
OH_2	3	top	15.99	−73.77
OH	7/2	top	40.79	−33.73
OH	7/2	bridge	40.77	−33.71
OH	7/2	cap	33.06	−26.00
O	2	cap	74.56	−17.72
O	2	bri	72.28	−15.44
O	2	top	27.00	−29.84

4.1.6. Application. We will use the following notation to clarify the type of heat of formation being discussed: ΔH_f refers to experimental heats of formation (298 K); δH_f refers to theoretical heats of formation (based on minimized energies without zero-point energy or temperature; and H_f refers to a combined heat of formation in which we start with CH_3OH and allow any extra Hs to be bound to the surfaces as isolated H_{ads}. To calculate the heat of formation of the CH_xO/M_8 clusters, we use the formula

$$\delta H_f(CH_xOy/Pt_8) = 627.5096\{E(CH_xO_y/M_8) - E_0(M_8) - E_0(C) - yE_0(O) - xE_0(H)\} \quad (12)$$

For example, the heat of formation of CH_2OH_{ads} is

$$\delta H_f(CH_2OH/Pt_8) = 627.5096\{-1068.41374 + 953.25726 + 38.13845 + 75.14908 + 3(0.58927)\} = -63.47 \text{ kcal/mol}$$

In comparing CH_xO clusters with various numbers of H atoms, we assume low coverage conditions in which excess H atoms end up at sites of the Pt surface well separated from the carbon- and oxygen-containing species. Thus, in examining rearranged structures starting with CH_3OH, we consider the combined H_f to be

$$\delta H_f(CH_xO/Pt_8) + (4 - x)\,\delta H_f(H/Pt_8) \quad (13)$$

For example, CH_2OH ($x = 3$) has one hydrogen less than CH_3OH, leading to $(4 - x) = 1$. Therefore, we add one increment of $\delta H_f(H/Pt_8)$ to account for the heat of formation for the chemisorbed H. For example, this leads to

$$H_f(CH_2OH) = \delta H_f(CH_2OH)_{ads} + \delta H_f(H_{ads}) = -63.47 - 11.38 = -74.85 \text{ kcal/mol}$$

The combined heats of formation are shown in Table 7.

4.2. Methanol Dehydrogenation on Pt. The complete dehydrogenation of methanol yields $(CO)_{ads}$ and four H_{ads}. We calculated the various likely intermediates in this reaction, obtaining the low-energy structures shown in Figure 3. The spin

(49) Chase, M. W., Jr.; Davies, C. A.; Downey, J. R., Jr.; Frurip, D. J.; McDonald, R. A.; Syverud, A. N. *J. Phys. Chem. Ref. Data, Suppl. 1* **1985**, *14*, 1.

(50) Christmann, K.; Ertl G.; Pignet, T. *Surf. Sci.* **1976**, *54*, 365.

(51) Engstrom, J. R.; Tsai, W.; Weinberg, W. H. *J. Chem. Phys.* **1987**, *87*, 3104.

(52) Conrad, H.; Ertl, G.; Latta, E. E. *Surf. Sci.* **1974**, *41*, 435.

(53) Yates, J. T., Jr.; Thiel, P. A.; Weinberg, W. H. *Surf. Sci.* **1979**, *84*, 427.

(54) Feulner, R.; Menzel, D. *Surf. Sci.* **1985**, *154*, 465.

Table 5. Optimized OH_x Ground Spin States

fragment	spin
OH_2	0
OH	1/2
O	1

Table 6. Calculated Energies, Heats of Formation, and Spin States of CO_2H_x/Pt_8 Clusters and Optimized CO_2H_x Ground Spin States

(a) Calculated Energies, Heats of Formation, and Spin States of CO_2H_x/Pt_8 Clusters

adsorbate on Pt_8	spin	site	binding energy (kcal/mol)	δH_f (kcal/mol)
HCOOH	3	top[a]	7.65	−94.89
$C(OH)_2$	2	top	72.85	−119.25
COOH	5/2	top	63.49	−106.28
CO_2	3	top	0.00	−90.70

b. Optimized CO_2H_x Ground Spin States

fragment	spin	fragment	spin
HCOOH (H-trans)	0	CO_2	0
COOH (trans)	1/2	$C(OH)_2$	0

[a] Carbonyl oxygen to surface. [b] Addition of calculated total energies of fragment and Pt_8 ($S = 3$).

Table 7. Combined Heats of Formation (kcal/mol) of CHO_x/M_8

adsorbate	Pt_8	Ir_8	Os_8	Pd_8	Rh_8	Ru_8
CH_3OH	−63.40	−57.53	−51.69	−54.77	−63.72	−54.03
OCH_3	−35.00	−42.46	−46.11	−49.73	−45.13	−42.98
CH_2OH	−74.85	−68.56	−63.84	−62.65	−65.61	−56.29
CH_2O	−55.70	−65.47	−61.93	−57.92	−68.10	−58.24
CHOH	−76.04	−72.70	−64.03	−74.17	−61.85	−55.92
CHO	−80.39	−78.23	−72.25	−67.33	−82.14	−61.67
COH	−96.24	−88.98	−81.99	−75.18	−81.78	−71.45
CO	−101.16	−96.92	−93.81	−108.73	−99.23	−85.53

Table 8. Combined Heats of Formation (kcal/mol) of OH_x/M_8

adsorbate	Pt_8	Ir_8	Os_8	Pd_8	Rh_8	Ru_8
OH_2	−73.77	−67.78	−63.56	−66.11	−69.47	−61.70
OH	−45.11	−42.99	−55.69	−51.22	−44.63	−53.63
O	−40.48	−57.59	−56.87	−52.50	−58.15	−69.92

state, site preference, total energy, and binding energy for each structure are listed in Table 2. Binding energies were calculated with respect to the naked Pt_8 ($S = 3$) cluster and the optimized fragments listed in Table 3. The energies of CH_x species and their corresponding binding energies to Pt_8 from our previous calculations of CH_x on Pt_8[36] are shown in Table 10.

Figure 4 displays the heat of formation chart for this reaction. For Pt each step of the dehydrogenation of methanol is exothermic all the way to formation of $(CO)_{ads}$. Indeed it is observed experimentally that CH_3OH rapidly dehydrogenates over Pt to form $(CO)_{ads}$.[17]

Stripping the hydrogens off the carbon leads to adsorbed intermediates that are more stable than losing the hydrogen off the oxygen. Thus, $(CH_2OH)_{ads}$ is more stable than $(OCH_3)_{ads}$, $(CHOH)_{ads}$ is more stable than $(CH_2O)_{ads}$, and $(COH)_{ads}$ is more stable than $(CHO)_{ads}$.

4.2.1. $(CH_3OH)_{ads}$. We calculate that CH_3OH_{ads} prefers to bind to the on-top site via the oxygen lone pair of electrons. Thus, the COH plane is tilted by 61° from the perpendicular (a tetrahedral lone pair would lead to 54.75°) and the Pt−O bond of 2.36 Å is longer than that for $(OCH_3)_{ads}$, which is 1.99 Å.

The calculated bond energy is 15.0 kcal/mol, which can be compared to the calculated bond energy of 16.0 kcal/mol for H_2O (same site). The experimental result for H_2O is 12 kcal/mol,[27] suggesting that our values are ∼4 kcal/mol too strong (as expected by our neglect of zero-point energy and vibrational enthalpy effects). Our calculated bond energy leads to $H_f(CH_3OH)_{ads} = -63.40$ kcal/mol.

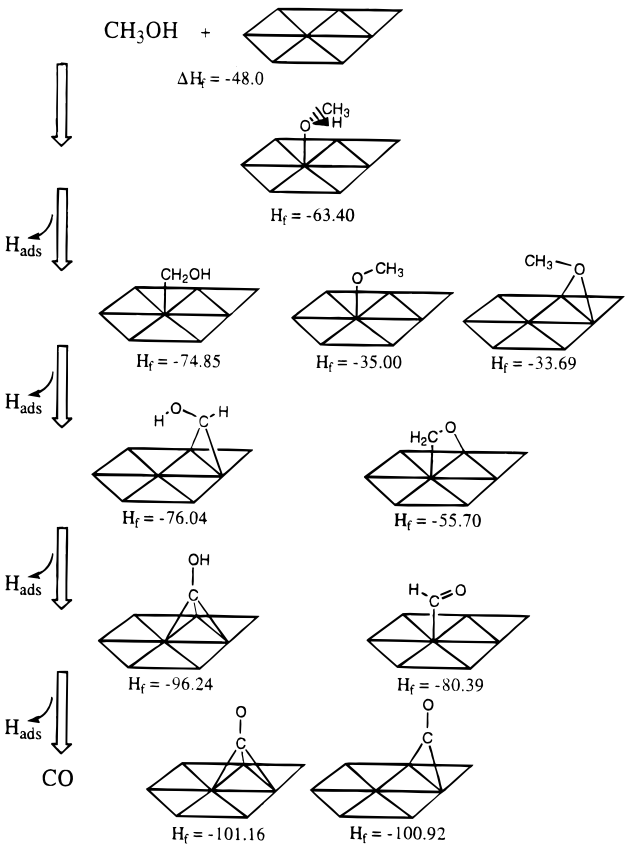

H_f listed includes H_f (H_{ads}) = -11.38 kcal/mol

a. heat of formation and binding site

CH_3OH	CH_2OH	OCH_3 (top)	OCH_3 (bridge)
• Pt-O 2.36 Å • C-O 1.44 Å • C-O-Pt 119°	• Pt-C 2.13 Å • C-O 1.35 Å • O-C-Pt 113°	• Pt-O 1.99 Å • C-O-Pt plane 119°	• Pt-O 2.28 Å [2] • C-O-Pt plane 127°
CHOH	CH_2O	COH	CHO
• Pt-C 2.07 Å [2] • C-O 1.33 Å • O-C-Pt plane 120°	• Pt-C 2.06 Å • Pt-O 2.31 Å • C-O 1.35 Å • C-O bond twisted 28° to Pt-Pt bridge	• Pt-C 1.96 Å [3] • C-O 1.33 Å • H-O-C 110° (staggered)	• Pt-C 2.01 Å • C-O 1.18 Å • O-C-Pt 126° • H-C-Pt 107°
CO (cap)	CO (bridge)		
• Pt-C 2.04 Å [2] Pt-C 2.16 Å • C-O 1.18 Å	• Pt-C 2.00 Å [2] • C-O 1.17 Å		

[indicates number of equivalent bonds (all within 0.01 Å)]

b. selected geometric parameters

Figure 3. Low-energy structures of CH_xO/Pt_8.

4.2.2. $(CH_2OH)_{ads}$ and $(OCH_3)_{ads}$. 4.2.2a. $(OCH_3)_{ads}$. We calculate that OCH_3 prefers the top site of Pt_8, leading to a covalent Pt−O bond length of 1.99 Å and a C−O−Pt angle of 119°. The bond energy is 25.04 kcal/mol, which is only 1.3 kcal/mol stronger than that for the bridge site (which has a bond length 0.29 Å longer).

The calculated bond energy leads to $H_f(OCH_3)_{ads} = -35.00$ kcal/mol. This is 63.40 − 35.00 = 27.6 kcal/mol endothermic from $(CH_3OH)_{ads}$, making this an unlikely intermediate (see Table 7).

4.2.2b. $(CH_2OH)_{ads}$. We calculate that CH_2OH has a bond energy of 65.7 kcal/mol to the on-top site with Pt−C = 2.13 Å and a tilt angle to the surface of 68°. The Pt−C bond distance

Table 9. Combined Heats of Formation (kcal/mol) on M_8

adsorbate	Pt_8	Ir_8	Os_8	Pd_8	Rh_8	Ru_8
$[CH_3OH]_g + [OH_2]_g$	−105.8	−105.8	−105.8	−105.8	−105.8	−105.8
$CH_3OH + OH_2$	−137.17	−125.31	−115.25	−120.88	−133.19	−115.73
$OCH3 + OH_2 + H$	−108.77	−110.24	−109.67	−115.84	−114.60	−104.68
$CH_2OH + OH_2 + H$	−148.62	−136.34	−127.40	−128.76	−135.08	−117.99
$CH_2O + OH_2 + 2H$	−129.47	−133.25	−125.49	−124.03	−137.57	−119.94
$CHOH + OH_2 + 2H$	−149.81	−140.48	−127.59	−140.28	−131.32	−117.62
$CHO + OH_2 + 3H$	−154.16	−146.01	−135.81	−133.44	−151.61	−123.37
$COH + OH_2 + 3H$	−170.01	−156.76	−145.55	−141.29	−151.25	−133.15
$CHO + OH + 4H$	−125.50	−121.22	−127.94	−118.55	−126.77	−115.30
$[HCOOH]_g + 4H$	−136.72[a]	−136.72[a]	−132.76	−132.76	−132.76[a]	−132.76
$COH + OH + 4H$	−141.35	−131.97	−137.68	−126.40	−126.41	−125.08
$C(OH)_2 + 4H$	−164.77	−162.95	−159.16	−151.79	−151.83	−146.83
$CO + OH_2 + 4H$	−174.93	−164.70	−157.37	−174.84	−168.70	−147.23
$CHO + O + 5H$	−120.87	−135.82	−129.12	−119.83	−140.29	−131.59
$COH + O + 5H$	−136.72	−146.57	−138.86	−127.68	−139.93	−141.37
$CO + OH + 5H$	−146.27	−139.91	−149.50	−159.95	−143.86	−139.16
$COOH + 5H$	−163.18	−160.91	−160.09	−156.97	−168.33	−157.57
$CO + O + 6H$	−141.64	−154.51	−150.68	−161.23	−157.38	−155.45
$[CO_2]_g + 6H$	−158.98	−158.98	−158.98	−158.98	−158.98	−158.98

[a] $H_f[(HCOOH)_{ads}]$ is −140.41, −136.72, and 142.17 kcal/mol for carbonyl oxygen bound to on-top Pt, Ir, and Rh.

Table 10. Calculated Energies, Heats of Formation, Spin States, and Pt−C Bond Distances of CH_x/Pt_8 Clusters[a]

adsorbate on Pt_8	spin	site	binding energy (kcal/mol)	Pt−C (Å)
CH_3	5/2	top	53.77	2.07
CH_2	2	bridge	104.28	2.01
CH	5/2	cap	166.60	1.95

[a] Reference 36.

in $(CH_2OH)_{ads}$ is longer (2.13 Å) than that in $(CH_3)_{ads}$ (2.07 Å), but the bond energy is 11.8 kcal/mol stronger. The increase in bond length might be due to steric interactions of the OH with the surface; we believe that the increase in bond strength must be an electronic effect (the OH polarizing the Pt−C bond to make it stronger).

The energetics lead to $H_f(CH_2OH)_{ads} = -74.85$ kcal/mol, making this process exothermic by 11.5 kcal/mol. Thus, forming $(CH_2OH)_{ads}$ is 40 kcal/mol more favorable than forming $(OCH_3)_{ads}$.

We have calculated the reaction path for dissociative chemisorption of CH_4 on Pt_8 to involve a transition state very similar to that found for $CH_4 + Pt(PH_3)_2 \rightarrow Pt(CH_3)(H)(PH_3)_2$,[55] which leads to simultaneous formation of the Pt−H and Pt−C bonds. We believe that CH_3OH probably involves a similar transition state.

4.2.3. $(CH_2O)_{ads}$ and $(CHOH)_{ads}$. 4.2.3a. $(CH_2O)_{ads}$. We calculate that CH_2O forms a di-σ bond to a bridge site with Pt−C = 2.06 Å and Pt−O = 2.01 Å. This is analogous to the di-σ bond of C_2H_4 to Pt_8. However, we find that di-σ CH_2O is bound by only 9.6 kcal/mol, whereas we find that di-σ C_2H_4 binds by 36.1 kcal/mol,[36] which is consistent with the most accurate experimental values ranging from 29.6 to 41.6 kcal/mol at low coverage using collision-induced desorption (CID)[56] and microcalorimetry.[57]

The weak bond of (di-σ $CH_2O)_{ads}$ is expected. Thus assuming a Pt−C bond strength of 48.6 kcal/mol (from C_2H_5/Pt_8),[36] the calculated bond energy of 36.1 for (di-σ $C_2H_4)_{ads}$ suggests a C_2H_4 π bond of 2(48.6) − 36.1 = 61.1 kcal/mol, a plausible value (the rotational barrier in C_2H_4 is ∼67 kcal/mol). Using bond energies of $D_{Pt-C} = 65.7$ (from CH_2OH/Pt_8) and $D_{Pt-O} =$ 25.0 kcal/mol (from OCH_3/Pt_8), the di-σ CH_2O bond energy of 9.6 kcal/mol suggests a π bond for CH_2O of 65.7 + 25.0 − 9.6 = 81.1 kcal/mol, which is higher than that of the C_2H_4 π bond by 20 kcal/mol.

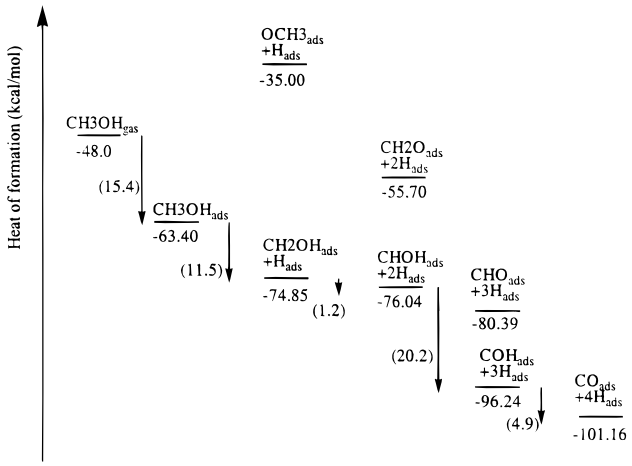

Figure 4. Heat of formation chart for methanol dehydrogenation on Pt.

These energetics lead to $H_f(CH_2O)_{ads} = -55.70$ kcal/mol, making this endothermic by 20 kcal/mol from $(CH_2OH)_{ads}$. However, CH_2O has been observed experimentally as one of the products of incomplete oxidation by in situ FTIR spectroscopy.[7]

4.2.3b. $(CHOH)_{ads}$. We find that CHOH binds to a bridge site (just as for CH_2) leading to tetrahedral carbon. The calculated bond energy is 20 kcal/mol more favorable for $CHOH_{ads}$ than (di-σ $CH_2O)_{ads}$. The calculated Pt−C bond length is 2.07 Å, which is 0.06 Å longer than that for CH_2, a plausible steric effect of the OH. The CHOH plane is perpendicular to the surface.

The calculated bond energy of 84.8 kcal/mol for $(CHOH)_{ads}$ is 19.5 kcal/mol weaker than that for $(CH_2)_{ads}$. This might seem strange since replacing an H of $(CH_3)_{ads}$ with OH increased the bond strength to the surface by 11.8 kcal/mol. However, the weaker CHOH bond is because the ground state of gas-phase CHOH is the singlet state (a Fischer carbene) with a doubly occupied σ lone pair whereas the binding state to the surface requires the two singly occupied orbitals of the CHOH triplet state (which we calculate to be 26.1 kcal/mol above the gas-

(55) Low, J. J.; Goddard, W. A., III *Organometallics* **1986**, *5*, 609.
(56) Szulczewski, G.; Levis, R. J. *J. Am. Chem. Soc.* **1996**, *118*, 325.
(57) Yeo, Y. Y.; Stuck, A.; Wartnaby, C. E.; King, D. A. *Chem. Phys. Lett.* **1996**, *259*, 28.

phase singlet). Thus the bond energy of the triplet to the surface is 84.8 + 26.1 = 110.9 kcal/mol, which is 6.6 kcal/mol stronger than the bond energy of CH_2 (which has a triplet ground state). We refer to such bond energy corrected to the proper dissociation product for forming the bond as a "snap bond energy". Here the geometry is optimized but the electronic state is fixed.

This leads to $H_f(CHOH)_{ads} = 2(-11.38) + 31.56 - 84.84 = -76.04$ kcal/mol, making formation of $(CHOH)_{ads}$ on the surface from $(CH_2OH)_{ads}$ exothermic by 1.19 kcal/mol.

4.2.4. $(CHO)_{ads}$ and $(COH)_{ads}$. 4.2.4a. $(CHO)_{ads}$. We find that $(CHO)_{ads}$ prefers the on-top site, with a bond energy of 62.7 kcal/mol and a Pt−C bond length of 2.01 Å.

Thus, $H_f(CHO)_{ads} = -80.39$ kcal/mol, which is 5 kcal/mol exothermic from $(CHOH)_{ads}$. We see below that forming $(COH)_{ads}$ is more exothermic by 21 kcal/mol. Even so, it is plausible that the O−H bond of $(CHOH)_{ads}$ might break first to form $(CHO)_{ads}$. This is because CHOH trans is structurally compatible with easy dehydrogenation from the oxygen, which might lead to a lower activation energy. Rearrangement to form the more stable $(COH)_{ads}$ could occur subsequently.

4.2.4b. $(COH)_{ads}$. We find that COH binds to the cap site (η^3) just as calculated for the analogous CH. The Pt−C bond lengths are similar, 1.96 and 1.95 Å, respectively, showing the covalent character (the CO bond is perpendicular to the surface, just as is the CH bond).

However, COH has a binding energy of 121.2 kcal/mol, much weaker than CH with a binding energy of 166.6 kcal/mol. This is expected since forming three covalent bonds to the Pt surface requires the three unpaired orbitals (σ, π_x, and π_y) of the quartet ($S = 3/2$) state of CH or COH, whereas the ground state is the doublet state ($S = 1/2$) with one unpaired π orbital. The adiabatic excitation energies from the $S = 1/2$ to 3/2 states are calculated to be 87.6 (COH) and 19.7 kcal/mol (CH), respectively. This leads to a "snap" binding energy of 208.8 kcal/mol for COH and 186.3 kcal/mol for CH. Thus OH strengthens the surface bond of CX by 22.5 kcal/mol, compared to 6.8 kcal/mol for CHX and 11.8 kcal/mol for CH_2X.

This leads to $H_f(COH)_{ads} = -96.24$ kcal/mol, which is 21 kcal/mol exothermic from $(CHOH)_{ads}$, making $(COH)_{ads}$ a likely intermediate.

4.2.5. $(CO)_{ads}$. Our calculations indicate that CO binds strongest to the cap site with the bridge site only 0.24 kcal/mol higher. We calculate the binding energy for $(CO)_{ads}$ to be 41.9 kcal/mol, which compares well with the best experimental values of 43 kcal/mol. Although we label it "cap" because structurally it resides in the 3-fold site, there are two strong Pt−C bonds (2.04 Å each) and one long Pt−C bond (2.16 Å). Hence, in terms of bonding, it is closely related to the bridge site. The CO bond distance of $(CO)_{ads}$ is 1.18 Å, which is 0.04 Å longer than that for $(CO)_{gas}$ and 0.15 Å shorter than that for $(COH)_{ads}$.

Since $H_f(CO)_{ads} = -101.16$ kcal/mol, losing the last H from $(COH)_{ads}$ is exothermic by 101.2 − 96.2 = 5.0 kcal/mol, making $(CO)_{ads}$ the thermodynamic sink in this reaction.

4.2.5a. Comparison to Experimental Binding Energies. Early experiments for CO on Pt(111) using temperature-programmed desorption (TPD)[58] reported a binding energy of 35 kcal/mol. TPD measurements are generally for higher coverage and for which assumptions are often made about the preexponential factors to derive an activation energy. Coverage-dependent microcalorimetry provides the most reliable and direct measure of the intrinsic bond energy. Recent experiments using microcalorimetry[28] report a value of 43 kcal/mol for low coverage, which drops to a steady state value of 28 kcal/mol for half monolayer coverage, and finally to 16 kcal/mol at high coverage. This low coverage value of 43 kcal/mol is in good agreement with our calculated value of 41.9 kcal/mol.

From slab calculations, Norskov and co-workers suggest the heat of adsorption of CO can be related to the position of the d-band of the Pt atop-atom relative to the Fermi energy.[35] Bonding arises from the interaction between the metal d states and the CO $2\pi^*$ and 5σ states. In addition, renormalization of the CO states arises via interaction with half-filled s-bands at the Pt(111) surface. The s^1d^9 electronic configuration of our cluster also corresponds to a half-filled s-band. Our model suggests that the interstitial orbitals formed by bonding interactions of the Pt 6s orbitals are very stable, and hence the density of electrons in the s-band is primarily at the base of the band. Although s−d mixing is present in our cluster, it does not form an s-band as diffuse as found in the slab calculations, which correspondingly changes the renormalization effect. It has been suggested that M_n clusters (where $n > 6$) show metallic character in the density of states. Dumesic and co-workers, studying CO binding to a Pt_{10} cluster, have compared the density of states to Norskov's slab calculations and concluded that the source of bonding is quite similar.[34]

The differences in binding energies due to computational methodology (basis sets, density functionals, slab thickness, size of cluster) have not been directly compared. However, the two different experimental numbers for CO adsorption correspond well to the two different numbers obtained by the slab and cluster approaches. The TPD result (35 kcal/mol) corresponds to the high coverage situation of the c(4 × 2) unit cell. The calculated slab binding energy with a p(2 × 2) unit cell of 34 kcal/mol matches this number. Both correspond to a quarter monolayer coverage. The cluster calculations (by both Dumesic's group and our group) on the other hand match the low coverage value that comes from the initial heat of adsorption measured by microcalorimetry.

For CO/Pd(111) no microcalorimetry has been reported, but TPD data[59−61] lead to 30−35 kcal/mol. A very recent slab calculation[62] at two different coverages on Pd(111) gives 33 kcal/mol for the c(2 × 2) structure [higher coverage] and 46 kcal/mol for the ($\sqrt{3} \times \sqrt{3}$) structure [lower coverage]. Our calculated number on CO/Pd_8 cluster is 49 kcal/mol, in reasonable agreement with the low coverage value.

For CO/Rh(111) no microcalorimetry has been reported. However, a very recent slab calculation,[63] at a lower coverage of p(3 × 3) CO/Rh(111), gives 41 kcal/mol, close to our cluster number of 39 kcal/mol. Here TPD data[61,64] lead to 31−32 kcal/mol.

We have not found microcalorimetry or slab calculations for the CO/Ru(0001) system. We do note that TPD[61,65] suggest a wide range of values from 28 to 38 kcal/mol. Our calculated number of 26 kcal/mol is at the lower end of this range, which may suggest that our bond energy for Co/Ru(0001) is too low by up to 10 kcal/mol. If our calculated numbers for Ru are on the low side (due to the basis set, the cluster, or the DFT functionals), this difference is expected to be *systematic* across

(58) Steininger, H.; Lehwald, S.; Ibach, H. *Surf. Sci.* **1982**, *123*, 264.
(59) Voogt, E. H.; Coulier, L.; Gijzeman, O. L. J.; Geus, J. W. *J. Catal.* **1997**, *169*, 359.
(60) Conrad, H.; Ertl, G.; Kuppers, J. *Surf. Sci.* **1978**, *76*, 323.
(61) Castner, D. G.; Sexton, B. A.; Somorjai, G. A. *Surf. Sci.* **1978**, *71*, 519.
(62) Loffreda, D.; Simon, D.; Sautet, P. *Surf. Sci.* **1999**, *425*, 680.
(63) Zhang, C. J.; Hu, P.; Lee, M.-H. *Surf. Sci.* **1999**, *432*, 305.
(64) Thiel, P. A.; Williams, E. D.; Yates, J. T., Jr.; Weinberg, W. H. *Surf. Sci.* **1979**, *84*, 54.
(65) Pfnur, H.; Feulner, P.; Menzel, D. *J. Chem. Phys.* **1983**, *79*, 4613.

all the Ru numbers. This will *not* change the conclusions since the relative numbers remain the same.

Summarizing, the experimental TPD numbers correspond to higher coverage conditions while our cluster numbers correspond to low coverages. Where available our results are confirmed by low-coverage experiment or lower coverage slab calculations.

4.2.5b. Comparison to Experimental Bonding Sites. Experimental studies of binding site have mainly used low-energy electron diffraction (LEED),[66] infrared reflection absorption spectroscopy (IRAS),[67] scanning tunneling microscopy (STM),[68] and sum frequency generation.[69] These experiments are generally interpreted in terms of CO chemisorbed mainly at on-top sites at low coverage, and on both on-top and bridge sites at higher coverages. However, there are no direct experimental results on the structure for the lowest coverages.

Slab calculations have only investigated bonding of CO to the on-top site. The difference we calculate between these sites (16.9 kcal/mol) seems rather large. Dumesic's group also finds a large difference (15.5 kcal/mol). Although the numbers match closely, their cluster does not have a net s^1d^9 configuration and is not optimized for spin. They have only investigated edge site terminal binding of CO. We could find no experimental evidence at low temperatures quantifying energetic site preference of CO on Pt(111), although it is commonly believed that the energy gap should be smaller. It would be useful to further investigate these effects by performing slab calculations with similar functionals and basis sets for direct comparison with the cluster calculations.

Using in situ FTIR and electrochemical mass spectrometry, Munk et al.[17] suggest that linearly bonded CO is formed initially at terrace sites on 15 nm Pt particles that subsequently migrate to edge or kink sites with increasing potential. The vacancies are then filled up by the transformation of singly bonded CO to triply bonded CO (in the 3-fold site). This migration was also observed on bulk polycrystalline metal, but with less pronounced effects since the relative terrace areas are larger.

We interpret these results as follows. At the high coverage usually used in experimental studies of structure and specific binding site, packing effects lead to on-top binding of CO, but at low coverage the strongest bond is to cap sites (as in our calculations). Thus removing sufficient CO from a saturated terrace allows the remaining adsorbed CO to change from on-top to cap. (We calculate the bridge site to be 0.24 kcal/mol higher than cap and on-top sites to be 16.9 kcal/mol higher.)

4.3. Dehydrogenation of Water on Pt. Complete dehydrogenation of water yields atomic O_{ads} and two H_{ads}. The spin state, site preference, total energy, and binding energy for each of the intermediates are listed in Table 4. The adsorbate structures are shown in Figure 5. Binding energies are calculated with respect to the naked Pt_8 ($S = 3$) cluster and the optimized OH_x fragments listed in Table 5.

The heat of formation for each of the Pt_8-OH_x clusters is calculated according to the same scheme as used above for the CH_xO adsorbates. The corrected heats of formation are given in Table 8. As above, we use $\delta H_f(H_{ads}) = -11.38$ kcal/mol. From the heat of formation chart (Figure 6), we see that dehydrogenation of water on Pt_8 is thermodynamically uphill by 28.7 kcal/mol for $(H_2O)_{ads} \rightarrow H_{ads} + (OH)_{ads}$. This is consistent with experiment since electrochemical experiments show that pure Pt decomposes water only at a high potential of 0.8 V vs RHE.

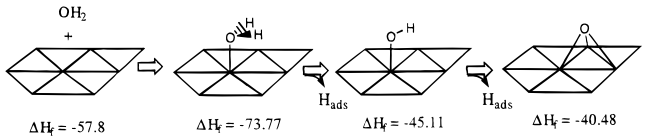

ΔH_f listed includes ΔH_f (H_{ads}) = -11.38 kcal/mol

a. heat of formation and binding site

OH_2	OH	O
• Pt-O 2.35 Å • O-H 0.973 Å [2] • H-O-H 105° • tilt of H_2O plane to perpendicular 81°	• Pt-O 1.97 Å • O-H 0.975 Å • H-O-Pt 103°	• Pt-O 1.96 Å [3]

[indicates number of equivalent bonds (all within 0.01 Å)]

b. selected geometric parameters

Figure 5. Low-energy structures of OH_x/Pt_8.

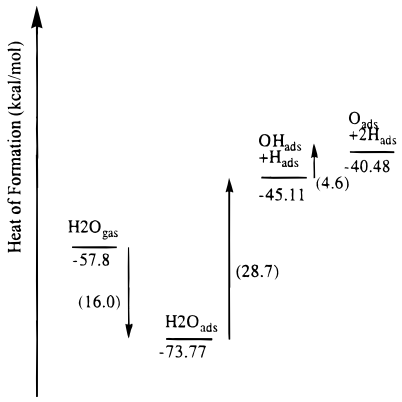

Figure 6. Heat of formation chart for water dehydrogenation on Pt.

4.3.1. $(H_2O)_{ads}$. We find that H_2O prefers the on-top site with a Pt−O bond length of 2.35 Å (cf. 2.36 Å for CH_3OH) and a tilt angle of 81° with respect to the vertical (cf. 61° for CH_3OH). Our calculated binding energy of 16.0 kcal/mol is comparable to the experimental adsorption energy of 12 kcal/mol.[27] We find that H_2O does not bind to the on-top and bridge sites.

For Ru, we calculate the adsorption energy of H_2O to be 4 kcal/mol. This compares with the TPD experimental number of 12 kcal/mol at low coverage.[67] This coincides with Pt where the TPD result is also 12 kcal/mol. We believe that the discrepancy for Ru may be because some amount of water dissociation takes place on Ru. Our calculations suggest that thermodynamics favors this by an additional 8 kcal/mol (see Section 5.2 and Figure 10). [This is not expected in Pt since the process is endothermic.] For high coverage conversion to multilayers of H_2O, TPD indicates a bond energy of 11.5 kcal/mol for Ru[67] and 12 kcal/mol for Pt.[27] We expect the multilayer ice peaks to appear in the same temperature range for both Ru and Pt. The energy should be ~12 kcal/mol since this is the heat of sublimation of normal ice.

4.3.2. $(OH)_{ads}$. We find that OH binds to the on-top site with a bond distance of 1.97 Å and a H−O−Pt angle of 103°. Our calculated binding energy is 40.8 kcal/mol, which compares to the experimental value of 47 kcal/mol.[29] Thus we calculate that forming $(OH)_{ads}$ from $(H_2O)_{ads}$ is endothermic by 28.7 kcal/mol. Adsorption of OH to the bridge and cap sites weakens the binding energy by 0.02 and 7.7 kcal/mol, respectively.

4.3.3. O_{ads}. We find that O binds to the cap site with a Pt−O bond distance of 1.96 Å. Our calculated binding energy is 74.6 kcal/mol, which compares to experimental values in the range

(66) Ogletree, D. F.; Van Hove, M. A.; Somorjai, G. A. *Surf. Sci.* **1986**, *173*, 351.

(67) Leung, L.-W. H.; Wieckowski, A.; Weaver, M. J. *J. Phys. Chem.* **1988**, *92*, 6985.

(68) Yau, S. L.; Gao, X.; Chang, S. C.; Schadt, B. C.; Weaver, M. J. *J. Am. Chem. Soc.* **1991**, *113*, 6049.

(69) Klunker, C.; Balden, M.; Lehwald, S.; Daum, W. *Surf. Sci.* **1996**, *360*, 104.

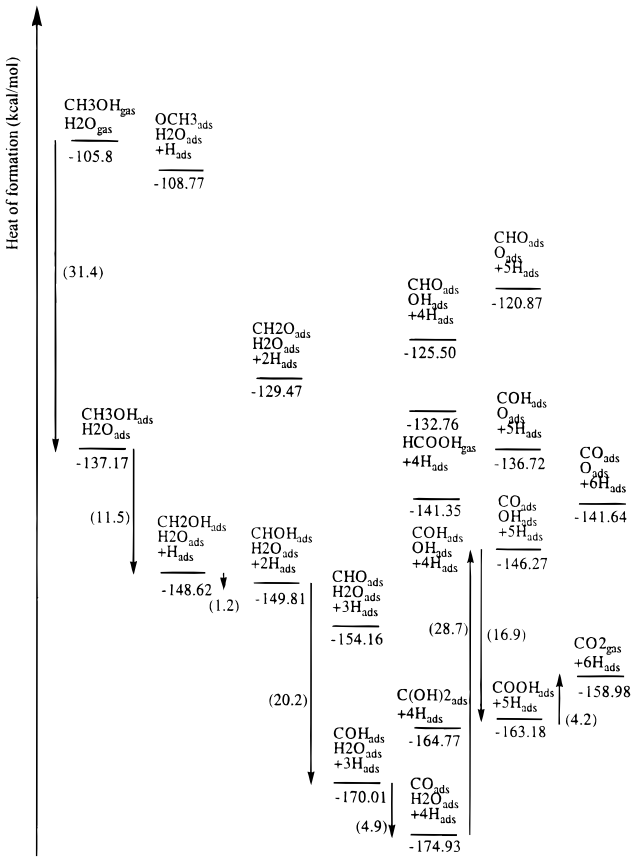

Figure 7. Combined heat of formation chart for methanol oxidation on Pt.

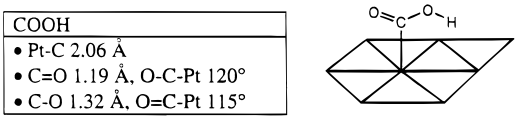

Figure 8. Structure of COOH/Pt_8.

of 40 to 110 kcal/mol.[71] Adsorption of O to the bridge and on-top sites weakens the binding energy by 2.3 and 47.5 kcal/mol, respectively. Since OH bonds to Pt with a bond energy of 40.8 kcal/mol, one might expect O_{ads} to have a bond energy of 81.6 kcal/mol. However, as discussed by Harding and Goddard,[72] the first bond to an O atom is weakened by ~8 kcal/mol because of loss of intraatomic exchange (e.g. The first bond of H to O is 111 kcal/mol whereas the 2nd is 119 kcal/mol). Thus it is plausible that the O bond to Pt is 7 kcal/mol weaker than twice that of OH.

4.3.4. Comparison to Other Calculations. First principles computational work in this area includes studying the binding of these species on Pt_4 and Pt_6 clusters (using nonlocal DFT). The calculated binding energies of H_2O, OH, and O are 8, 53, and 65 kcal/mol, respectively, in sites similar to our calculation.[73] Using nonlocal DFT with a triple-ζ basis set and a larger Pt_{10} cluster, O in the 3-fold site was calculated to have an adsorption energy of 66 kcal/mol.[74]

4.3.5. Other Intermediates. For the Pt_8 cluster, we find that COOH binds strongly (63.5 kcal/mol) but HCOOH weakly (8 kcal/mol through the oxygen lone pair), and no surface bond

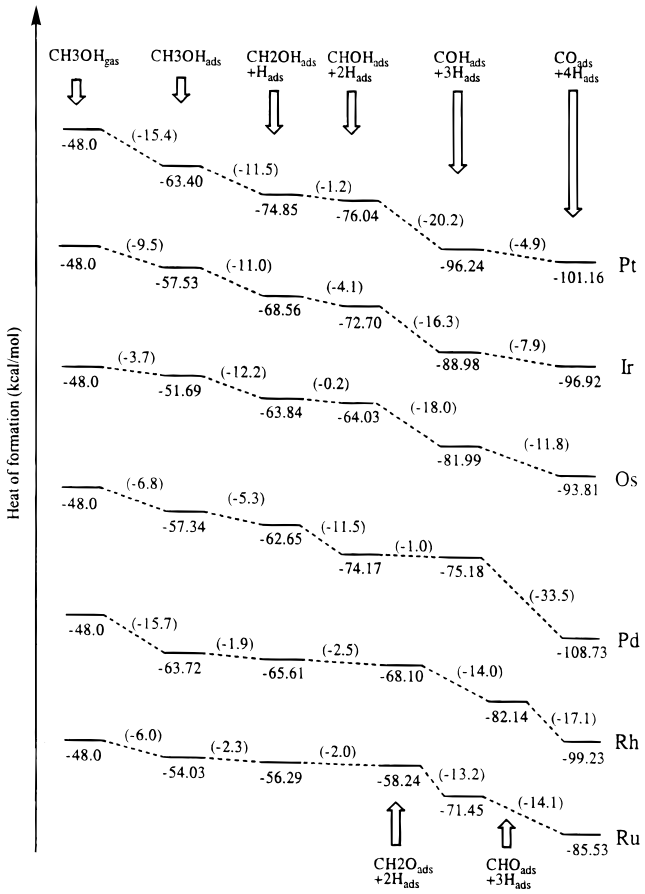

Figure 9. Heat of formation chart for comparing methanol dehydrogenation on Pt, Ir, Os, Pd, Rh, and Ru showing only the most stable isomers.

for CO_2. In section 4.2.3, we find that bridged CHOH binds 19.5 kcal/mol weaker than bridged CH_2. Thus, the effect of replacing H with an OH substituent is to reduce the surface bond energy by ~20 kcal/mol. Comparing the binding of CH_2O and HCOOH, we would expect the binding energy of HCOOH to be ~20 kcal/mol weaker. Since the binding energy of di-σ CH_2O is 9.6 kcal/mol, di-σ HCOOH is not expected to bind.

We find that formic acid, HCOOH, bonds through the carbonyl oxygen at the on-top site (Pt−O = 2.36 Å; C−O−Pt = 121°) by 8 kcal/mol. However, it does not form a π bond like $(CH_2O)_{ads}$. To make the π bond requires that the COO plane be parallel to the surface, which apparently causes steric interactions of the OH with the surface that are too large given the small value (~10 kcal/mol) expected for the bond.

Removing the H from HCOOH leads to $(COOH)_{ads}$, which bonds by 63.5 kcal/mol with a Pt−C bond length of 2.06 Å. This can be compared to 62.7 kcal/mol and 2.01 Å for $(CHO)_{ads}$.

Another important intermediate is the carbene $C(OH)_2$ that bonds to the on-top site by 72.9 kcal/mol with a Pt−C bond length of 1.92 Å. The bridge bond (Pt−C 2.23 Å) is less stable by 9.7 kcal/mol. For $(CH_2)_{ads}$, the bridge site is favored over the on-top site by 104.3 − 78.1 = 26.2 kcal/mol. For $(CHOH)_{ads}$, the bridge site is favored by only 84.8 − 79.7 = 5.1 kcal/mol. Hence, the effect of replacing H with an OH substituent is to stabilize the on-top site by 21.1 kcal/mol with respect to the bridge site. Thus, for the carbene $[C(OH)_2]_{ads}$ we expect the on-top site to be favored over the bridge site since CHOH at the bridge site is only 5.1 kcal/mol favored over the on-top site.

(70) Madey, T. M.; Yates, J. T., Jr. *Chem. Phys. Lett.* **1977**, *51*, 77.
(71) Gland, J. L.; Sexton, J. L.; Fisher, G. B. *Surf. Sci.* **1980**, *95*, 587.
(72) Harding, L. B.; Goddard, W. A., III *Annu. Rev. Phys. Chem.* **1978**, *29*, 363.
(73) Fahmi, A.; van Santen, R. A. *Z. Phys. Chem.* **1996**, *197*, 203.
(74) Chen, M.; Bates, S. P.; van Santen, R. A.; Friend, C. M. *J. Phys. Chem. B* **1997**, *101*, 10051.

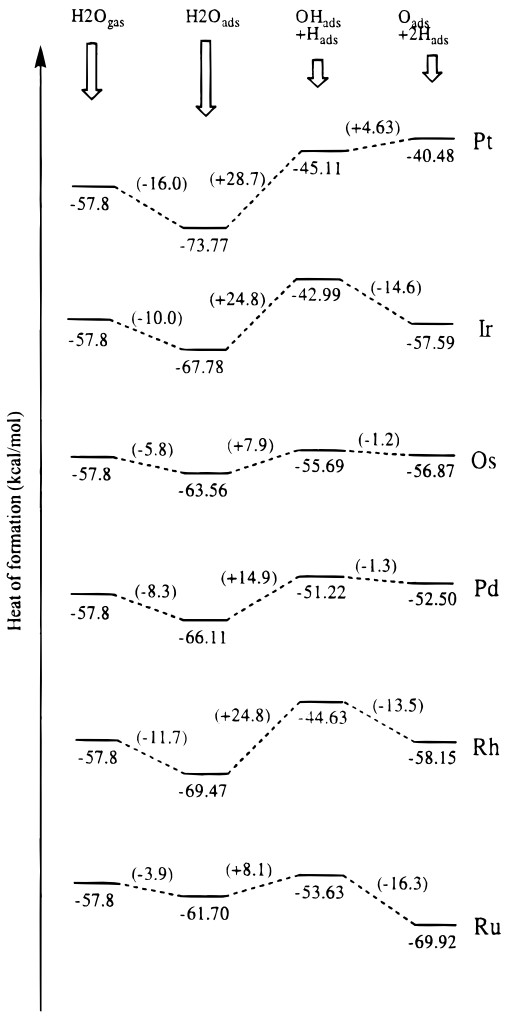

Figure 10. Heat of formation chart for comparing water dehydrogenation on Pt, Ir, Os, Pd, Rh, and Ru.

The results for these species are given in Tables 6a and 6b.

4.4. Combined Dehydrogenation and Oxidation on Pt. To examine the entire process, we combine the separate heat of formation charts (Figures 4 and 6) into one chart, with the addition of species that have formed the second C−O bond. Figure 7 shows the combined heat of formation chart. Compounds in the same *vertical column* are isomers. Corrected heats of formation are given in Table 9.

The first half of the pathway in Figure 7 suggests facile dehydrogenation of CH_3OH from the carbon end to yield first $(COH)_{ads}$ and then $(CO)_{ads}$. In the second half, we see that dehydrogenating water from the thermodynamic sink of $(CO)_{ads} + (OH_2)_{ads} + 4H_{ads}$ ($H_f = -174.93$ kcal/mol) to OH_{ads} is 28.7 kcal/mol uphill, and further dehydrogenation to O_{ads} requires another 4.6 kcal/mol. Directly transforming to $(COOH)_{ads} + 5H_{ads}$ ($H_f = -163.18$ kcal/mol) via simultaneous dehydrogenation and C−O bond formation would be uphill 11.8 kcal/mol.

Subsequent dehydrogenation of $(COOH)_{ads}$ to desorb CO_2 from the surface is expected to have a low barrier reaction because COOH is structurally compatible for the dehydrogenation (see Figure 8) (we calculate a barrier of 10 kcal/mol). Thus, we conclude that $(CO)_{ads} + (OH)_{ads}$ would combine to form $(COOH)_{ads}$ in a reaction downhill by 16.9 kcal/mol. Consequently, we do not expect the reaction to go through both $(CO)_{ads} + O_{ads}$ species. Due to the high potential required to dehydrogenate water on platinum, it has been suggested that the oxygen-active species is "activated" water. Our results suggest that this "active water" is $(OH)_{ads}$. This would subsequently form the second C−O bond which is less favorable thermodynamically than forming $(COOH)_{ads}$ directly from $(CO)_{ads}$ and $(OH_2)_{ads}$.

Forming the second C−O bond from $(COH)_{ads}$ and $(OH)_{ads}$ leads to $[C(OH)_2]_{ads}$ ($H_f = -164.77$ kcal/mol). This species could then easily dehydrogenate to form $(COOH)_{ads}$ ($H_f = -163.18$ kcal/mol) and H_{ads}, which is endothermic by 0.4 kcal/mol. However, starting from $(COH)_{ads} + (H_2O)_{ads}$ the reaction has to go uphill 28.7 kcal/mol to first form $(COH)_{ads} + (OH)_{ads}$ ($H_f = -141.35$ kcal/mol) before forming $[C(OH)_2]_{ads}$. Since stripping the hydrogens from methanol is facile on Pt, it is more likely that $(COH)_{ads}$ dehydrogenates to $(CO)_{ads}$ (downhill 4.9 kcal/mol) leading to the pathway discussed above that bypasses the formation of $[C(OH)_2]_{ads}$.

Table 11. Calculated Energies, Spin States, and Structural Information for CH_xO_y and OH_x on Ir_8

adsorbate on Ir_8	spin; site	binding energy (kcal/mol)	selected bond distances (Å)
CH_3OH	$S = 7$; top	9.08	Ir−O 2.50; C−O 1.43
OCH_3	$S = 15/2$; top	32.50	Ir−O 1.98; C−O 1.40
CH_2OH	$S = 13/2$; top	59.37	Ir−C 2.09; C−O 1.40
CH_2O	$S = 6$; bridge	19.39	Ir−C 2.06; C−O 1.43; Ir−O 2.01
CHOH	$S = 6$; bridge	81.50	Ir−C 2.10; C−O 1.35
CHO	$S = 13/2$; top	60.55	Ir−C 2.00; C═O 1.20
COH	$S = 13/2$;cap	113.89	Ir−C 1.97; C−O 1.34
CO	$S = 7$; bridge	37.63	Ir−C 2.01; C═O 1.18
OH_2	$S = 7$; top	9.98	Ir−O 2.44
OH	$S = 15/2$; top	44.26	Ir−O 1.98
O	$S = 7$; cap	91.66	Ir−O 1.96
HCOOH	$S = 7$; top	3.96	Ir−O 2.47
$C(OH)_2$	$S = 13$; top	71.03	Ir−C 1.95
COOH	$S = 13/2$; top	63.28	Ir−C 1.99; C═O 1.22; C−O 1.33

5. Methanol Oxidation on 2nd and 3rd Row Group VIII Transition Metals

The favorable methanol activation processes observed for transition metal alloys (both the familiar Pt−Ru and the recent ternary/quaternary systems involving Ir and Os) suggested that we investigate the various intermediates for methanol oxidation on Pt, Ir, Os, Pd, Rh, and Ru. Thus, we calculated the optimum structures and energetics of the intermediate species on a M_8 cluster using bulk M−M distances. As before, we considered three parts to the reaction: (1) methanol dehydrogenation, (2) water dehydrogenation, and (3) oxidation via formation of the second C−O bond. Heats of formation were calculated using the same scheme as for Pt using a uniform correction of $\delta H_f(H_{ads}) = -11.38$ kcal/mol.

The spin state, site preference, total energy, and binding energy for each of the intermediates on the other five M_8 clusters are given in Tables 11−15. In general, there is not much difference in binding site across the metals except for $(CO)_{ads}$. We find that Pt, Pd, Rh, and Ru prefer CO in the cap site, Ir in the bridge site, and Os in the top site. Our calculations find that HCOOH bonds only to Pt (7.95 kcal/mol), Ir (4.0 kcal/mol), and Rh (9.4 kcal/mol) while CO_2 does not bind to any of the metals. OCH_3 binds most strongly to the on-top site in all metals except Pd where it prefers the cap site. $(CH_3OH)_{ads} \rightarrow (CH_2O)_{ads} + 2H_{ads}$ is downhill by 10 kcal/mol for Os, 8 kcal/mol for Ir, and 4 kcal/mol for Ru, Rh, and Pd, but uphill by 8 kcal/mol for Pt. Di-σ CH_2O is favorable over CHOH by 11 kcal/mol for Rh and 2 kcal/mol for Ru, but is disfavored by 20 kcal/mol for Pt.

Table 12. Calculated Energies, Spin States, and Structural Information for CH_xO_y and OH_x on Os_8

adsorbate on Os_8	spin; site	binding energy (kcal/mol)	selected bond distances (Å)
CH_3OH	$S = 11$; top	3.25	Os−O 2.64; C−O 1.43
OCH_3	$S = 21/2$; top	36.16	Os−O 1.99; C−O 1.41
CH_2OH	$S = 19/2$; top	54.66	Os−C 2.12; C−O 1.41
CH_2O	$S = 10$; bridge	15.85	Os−C 2.11; C−O 1.43; Os−O 2.03
CHOH	$S = 10$; bridge	72.83	Os−C 2.12; C−O 1.36
CHO	$S = 21/2$; top	54.57	Os−C 2.00; C═O 1.23
COH	$S = 19/2$; cap	106.90	Os−C 2.03; C−O 1.35
CO	$S = 9$; top	34.53	Os−C 1.84; C═O 1.16
OH_2	$S = 11$; top	5.76	Os−O 2.52
OH	$S = 21/2$; top	51.35	Os−O 2.00
O	$S = 10$; cap	90.94	Os−O 1.99
$C(OH)_2$	$S = 10$	67.24	Os−C 1.99
COOH	$S = 21/2$; top	60.40	Os−C 2.03; C═O 1.23; C−O 1.34

Table 13. Calculated Energies, Spin States, and Structural Information for CH_xO_y and OH_x on Pd_8

adsorbate on Pd_8	spin; site	binding energy (kcal/mol)	selected bond distances (Å)
CH_3OH	$S = 1$; top	6.32	Pd−O 2.35; C−O 1.44
OCH_3	$S = 3/2$; cap	39.78	Pd−O 2.12; C−O 1.43
CH_2OH	$S = 3/2$; top	53.46	Pd−C 2.05; C−O 1.37
CH_2O	$S = 1$; bridge	11.84	Pd−C 1.95; C−O 1.34; Pd−O 2.00
CHOH	$S = 1$; bridge	82.97	Pd−C 2.05; C−O 1.34
CHO	$S = 1/2$; top	49.65	Pd−C 1.95; C═O 1.20
COH	$S = 3/2$; cap	114.02	Pd−C 1.95; C−O 1.32
CO	$S = 1$; cap	49.45	Pd−C 2.05; C═O 1.18
OH_2	$S = 1$; top	8.31	Pd−O 2.30
OH	$S = 3/2$; top	46.89	Pd−O 1.92
O	$S = 1$; cap	86.58	Pd−O 1.95
$C(OH)_2$	$S = 1$; top	59.88	Pd−C 1.90
COOH	$S = 1/2$; top	57.29	Pd−C 1.94; C═O 1.22; C−O 1.33

Table 14. Calculated Energies, Spin States, and Structural Information for CH_xO_y and OH_x on Rh_8

adsorbate on Rh_8	spin; site	binding energy (kcal/mol)	selected bond distances (Å)
CH_3OH	$S = 7$; top	15.28	Rh−O 2.51; C−O 1.43
OCH_3	$S = 15/2$; top	35.18	Rh−O 2.05; C−O 1.40
CH_2OH	$S = 13/2$; top	56.42	Rh−C 2.03; C−O 1.43
CH_2O	$S = 6$; bridge	22.02	Rh−C 2.05; C−O 1.39; Rh−O 1.99
CHOH	$S = 6$; bridge	70.66	Rh−C 2.04; C−O 1.35
CHO	$S = 13/2$; top	64.67	Rh−C 1.91; C═O 1.23
COH	$S = 13/2$; cap	106.69	Rh−C 1.96; C−O 1.34
CO	$S = 7$; cap	39.96	Rh−C 2.06; C═O 1.19
OH_2	$S = 7$; top	11.67	Rh−O 2.49
OH	$S = 15/2$; top	40.30	Rh−O 2.02
O	$S = 6$; cap	92.23	Rh−O 1.95
$C(OH)_2$	$S = 6$; top	59.91	Rh−C 1.91
COOH	$S = 13/2$; top	68.85	Rh−C 1.94; C═O 1.24; C−O 1.34

5.1. CH_3OH Dehydrogenation. The heat of formation chart of methanol dehydrogenation for all six metals is shown in Figure 9. Only the most stable isomers are shown. Quantitative details are shown in Table 7.

Overall, Pt is the most favorable for methanol dehydrogenation since its intermediate adsorbed species are generally more stable than for the other metals.

The least favorable pathway is for Ru, which has a roughly flat energy curve for the initial dehydrogenation and goes downhill only to lose the third and fourth hydrogen. This suggests that Ru is a poor metal for stripping hydrogens off the carbon in methanol. Thus it is not surprising that pure Ru leads to a dead catalyst for methanol oxidation.

Table 15. Calculated Energies, Spin States, and Structural Information for CH_xO_y and OH_x on Ru_8

adsorbate on Ru_8	spin; site	binding energy (kcal/mol)	selected bond distances (Å)
CH_3OH	$S = 11$; top	5.59	Ru−O 2.73; C−O 1.43
OCH_3	$S = 21/2$; top	33.03	Ru−O 1.94; C−O 1.41
CH_2OH	$S = 21/2$; top	47.10	Ru−C 2.08; C−O 1.43
CH_2O	$S = 10$; bridge	12.16	Ru−C 2.12; C−O 1.39; Ru−O 1.95
CHOH	$S = 10$; bridge	64.72	Ru−C 2.09; C−O 1.36
CHO	$S = 21/2$; top	44.06	Ru−C 1.98; C═O 1.22
COH	$S = 21/2$; cap	96.37	Ru−C 1.99; C−O 1.35
CO	$S = 10$; cap	26.25	Ru−C 2.10; C═O 1.20
OH_2	$S = 11$; top	3.91	Ru−O 2.75
OH	$S = 23/2$; top	49.30	Ru−O 2.00
O	$S = 10$; cap	104.00	Ru−O 1.96
$C(OH)_2$	$S = 10$; top	54.92	Ru−C 1.97
COOH	$S = 21/2$; top	57.89	Ru−C 1.99; C═O 1.24; C−O 1.34

Intermediate to Pt and Ru for methanol dehydrogenation are Ir, Pd, and Rh. All three follow a basic downhill trend for methanol dehydrogenation with a similar general pathway. Notable differences are that Rh prefers $(CH_2O)_{ads}$ over $(CHOH)_{ads}$; Pd makes $(CHO)_{ads}$ to be uphill from $(CHOH)_{ads}$, while $(COH)_{ads}$ follows the general downhill trend; and Os has a rather shallow curve for initial dehydrogenation (similar to Ru) but still goes downhill.

5.2. Water Dehydrogenation. For water dehydrogenation, the trends are opposite that observed for CH_3OH. The heat of formation chart for all six metals is shown in Figure 10; quantitative details are given in Table 8. In this case, Pt is poorest for dehydrogenation while Ru is the most facile. Ru is observed to have a much smaller potential (0.2 V vs RHE) for water decomposition and it is possible that atomic oxygen is the activated species for oxidation. For both Ir and Rh the first dehydrogenation is significantly uphill, followed by a downhill second dehydrogenation to form atomic O_{ads}. Pd and Os follow a similar trend with much shallower curves, Os being less steep.

These results support the bifunctional mechanism of Pt−Ru for methanol oxidation. Of the six metals, Pt is the most facile for methanol dehydrogenation because of its ability to easily strip hydrogens from the carbon. Dehydrogenating water, however, is more facile on Ru than the other five metals. Hence, the binary combination yielding the best overall activity for methanol oxidation is Pt−Ru.

5.3. Combined Results. Quantitative details for the combined heat of formation values are given in Table 9. Except for Os, none of the *pure* metals favor the complete methanol oxidation reaction. Pt, Ir, Pd, and Rh are favorable for methanol dehydrogenation (Pt is the best) but are poor for water dehydrogenation. Ru favorably dehydrogenates water but does poorly for methanol.

5.4. Pt + Ru. To analyze the effect of a Pt−Ru alloy, we combine the data for methanol dehydrogenation using Pt (1st column of Table 7) with the data for water dehydrogenation using Ru (6th column of Table 8). From Figure 11, we see that dehydrogenation still proceeds downhill (left half). However, the ability of Ru to decompose water changes the thermodynamics to form the second C−O bond.

Comparing Figure 11 with the combined data for pure Pt (Figure 7), we find that in Pt−Ru, the formation of $(COOH)_{ads}$ ($H_f = -163.18$ kcal/mol) directly from $(CO)_{ads} + (H_2O)_{ads} +$

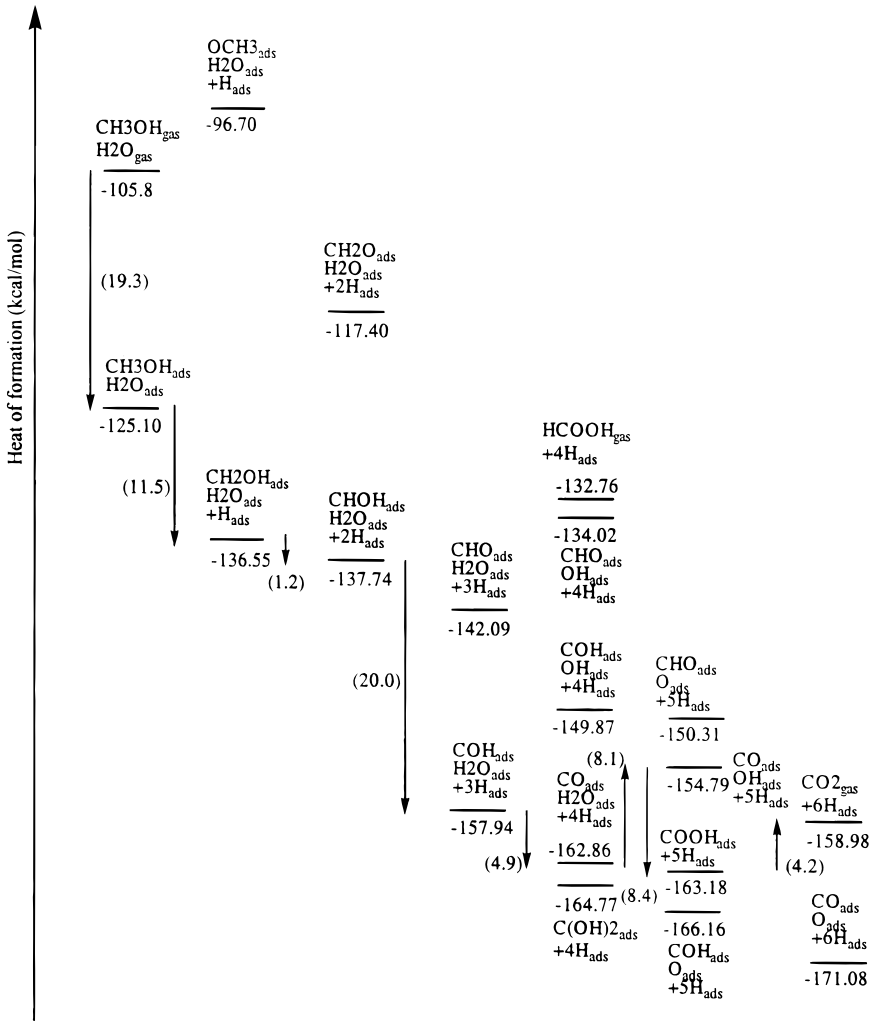

Figure 11. Combined heat of formation chart for methanol oxidation on Pt−Ru.

$5H_{ads}$ (H_f = −162.86 kcal/mol) is downhill by 0.3 kcal/mol. Were this to proceed sequentially by dehydrogenating water first to form $(CO)_{ads} + (OH)_{ads} + 5H_{ads}$ (H_f = −154.79 kcal/mol), it would have an initial uphill step of only 8.1 kcal/mol compared to 28.7 kcal/mol for pure Pt. A more probable pathway is via the formation of $(COH)_{ads} + O_{ads} + 5H_{ads}$ (H_f = −166.16 kcal/mol). This is more stable than $(CO)_{ads} + (H_2O)_{ads} + 5H_{ads}$ by 3.30 kcal/mol, and forming $(COOH)_{ads}$ from $(CO)_{ads} + (OH)_{ads}$ is only 3.0 kcal/mol uphill. Thus the most favorable pathway goes through different intermediates suggesting a different reaction mechanism for Pt−Ru than for pure Pt. Once again the last dehydrogenation step converting $(COOH)_{ads}$ to desorbed CO_2 is expected to have a low activation barrier. Although this chart indicates that $(CO)_{ads} + O_{ads}$ is the thermodynamic sink, we see that oxidation can occur before methanol is fully dehydrogenated. Thus because Ru does so well at activating water to $(OH)_{ads}$ (or O_{ads}), the $(CO)_{ads} + O_{ads}$ state need not be accessed.

5.5. Pure Os Case. Finally, pure Os provides an interesting balance of the two dehydrogenations. Although less capable of dehydrogenating methanol than Pt and of dehydrogenating water than Ru, Os can do both processes favorably. Figure 12 shows the combined heats of formation for Os. The reaction is downhill practically all the way to form desorbed CO_2. Forming $(COOH)_{ads} + 5H_{ads}$ (H_f = −160.09 kcal/mol) directly from $(CO)_{ads} + (H_2O)_{ads} + 4H_{ads}$ (H_f = −157.37 kcal/mol) is downhill 3.3 kcal/mol. If this step proceeds sequentially by first forming $(CO)_{ads} + (OH)_{ads} + 5H_{ads}$ (H_f = −149.50 kcal/mol), then this initial step is only 7.9 kcal/mol uphill. This is much more favorable than Pt (28.7 kcal/mol uphill) and even slightly more favorable than Pt−Ru (8.1 kcal/mol uphill). Once again the last dehydrogenation step converting $(COOH)_{ads}$ to desorbed CO_2 is expected to have a low activation barrier, and the reaction is only 1.1 kcal/mol uphill. The mechanism goes through intermediates similar to pure Pt (but different than Pt−Ru).

These results suggest that the role of Os as a promoter in the quaternary system may be 2-fold: it can contribute to dehydrogenation of methanol, but so can Pt and Ir (also a promoter), and it can activate the oxygen species (water or its dehydrogenated counterparts), which can be done by Ru but not Pt or Ir.

5.6. Kinetics. We have neglected the barriers for the various reaction steps. This is a serious limitation since the barriers dominate the rates. However, we expect somewhat similar results for the barriers for the same reaction steps on different metals. Thus, we believe that the energetics and structures allow us to reason reasonably well about the various mechanistic steps. Future work will examine barriers for the key steps in the reaction.

6. Conclusions

We examined the intermediates involved in the methanol oxidation reaction in DMFCs on the 2nd and 3rd row Group VIII transition metals. The overall reaction can be considered in three stages: (1) dehydrogenation of methanol, (2) dehydro-

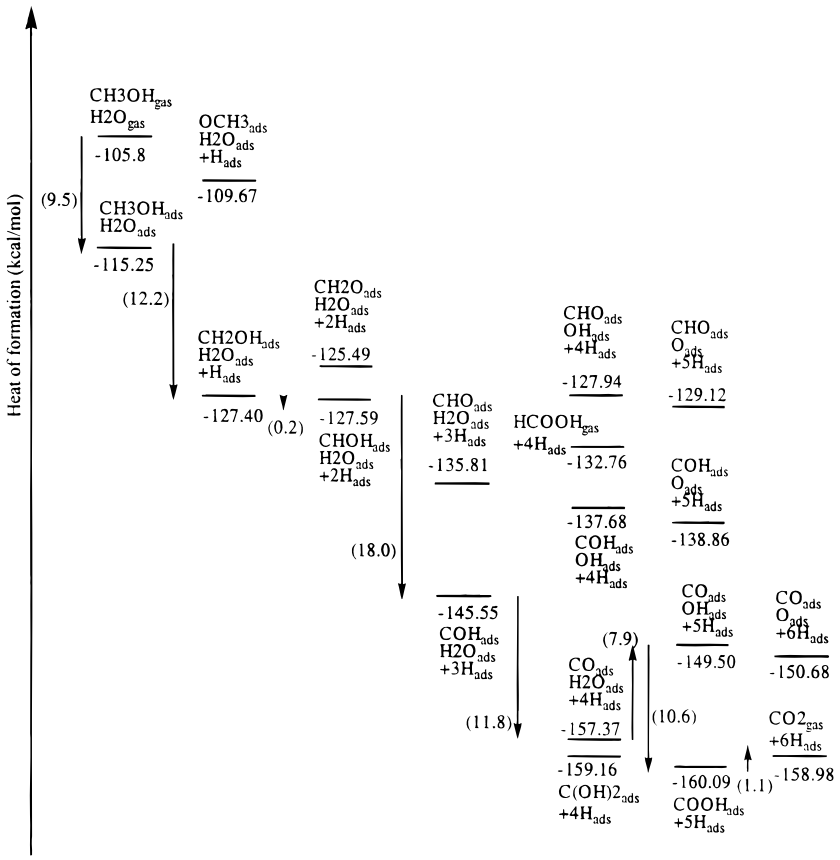

Figure 12. Combined heat of formation chart for methanol oxidation on Os.

genation of water, and (3) formation of the second C−O bond. For pure Pt, we find that $(CO)_{ads}$ is the thermodynamic sink in the reaction, in agreement with experimental evidence that this species poisons catalytic activity if not actively removed from the surface. We also find that of the six metals, methanol dehydrogenation is most facile on Pt, while Ir is also favorable for this reaction. The mechanism of methanol dehydrogenation proceeds via stripping of the hydrogens from the carbon end before the oxygen end.

For water dehydrogenation, Ru is the most active while Pt performs very poorly. These results support the bifunctional mechanism of Pt−Ru whereby Pt is responsible for the dehydrogenation of methanol and Ru for the dehydrogenation of water.

Our studies also suggest that Os, although poorer than Pt and Ru in their separate steps, combines both capabilities of the bifunctional mechanism. It is able to dehydrogenate both methanol and water favorably from a thermodynamic standpoint. This suggests that pure Os be examined as a potential DMFC catalyst. Although expensive it may lead to favorable kinetics even at very high dispersion and may have more favorable barriers (lower overpotential).

Our results suggest that $(COOH)_{ads}$ is likely the primary species obtained from forming the second C−O bond. In pure Pt, this species is formed via the reaction of CO_{ads} with $(OH)_{ads}$ [or $(H_2O)_{ads}$]. Pure Os follows this same pathway but it is more favorable thermodynamically. In Pt−Ru, a more favorable pathway can take place via the reaction $(COH)_{ads} + O_{ads}$. In either case the final step in the pathway is the dehydrogenation of $(COOH)_{ads}$ to desorb CO_2 from the surface.

Acknowledgment. We thank Professor Eugene Smotkin for helpful comments. This research was initiated with funding from NSF (CHE 95-22179) and continued with funding from ARO (in collaboration with Illinois Institute of Technology and Schrodinger Inc.). The facilities of the MSC are also supported by grants from DOE-ASCI, ARO/DURIP, ARO/MURI, BP Chemical, Beckman Institute, Seiko-Epson, Exxon, Owens-Corning, Avery-Dennison, Asahi Chemical, Chevron Petroleum Technology Co., Chevron Chemical Co., Chevron Research, and Technology Corp.

Supporting Information Available: Tables of absolute energies (PDF). This material is available free of charge via the Internet at http://pubs.acs.org.

JA9844074